BEARING CAPACITY OF FOOTINGS OVER TWO-LAYER FOUNDATION SOILS

By Radoslaw L. Michalowski,[1] Member, ASCE, and Lei Shi,[2] Student Member, ASCE

ABSTRACT: The bearing capacity of strip footings over a two-layer foundation soil is considered. The kinematic approach of limit analysis is used to calculate the average limit pressure under footings. The method is applicable to any combination of parameters of the two layers, but the results are presented only for a specific case when a footing is placed on a layer of granular soil resting on clay. The depth of the collapse mechanism is found to be very much dependent on the strength of the clay. Very weak clay can "attract" the mechanism even at great depths. The results are presented as limit pressures rather than traditional bearing-capacity coefficients. The latter are strongly dependent not only on the internal friction angle of the sand, but also on the thickness of the sand layer, cohesion of the clay, and surcharge pressure. Results are presented in the form of dimensionless charts for different internal friction angles of sand. It was found that linear interpolation within 5° increments is acceptable in the range of φ from 30° to 45°.

INTRODUCTION

The bearing capacity of footings comprises quite an extensive literature today. Most design methods are based on semiempirical formulas. The original Prandtl (1920) and Reissner (1924) solution to limit pressure on a strip punch over a perfectly plastic cohesive-frictional weightless half-space is usually altered to accommodate departure from symmetrical loads, to account for different footing shapes, and to include the resistance due to the soil weight (Hansen 1970). Either limit equilibrium considerations or an empirical approach is usually used to account for the conditions not included in the Prandtl-Reissner solution.

The methods for calculating the bearing capacity of multilayer soils range from averaging the strength parameter [cf. Bowles (1988)], using limit equilibrium considerations (Reddy and Srinivasan 1967; Meyerhof 1974), to a more rigorous limit analysis approach (Chen and Davidson 1973; Florkiewicz 1989). The finite-element method can capture the complexity of the boundary conditions and soil nonhomogeneity quite accurately, but it is more elaborate and has not found a wide acceptance in foundation design practice. The effort presented herein is restricted to finding the bearing capacity (or average limit pressure) on symmetrically loaded strip footings over a two-layer foundation soil. The method presented can be applied to any combination of two different soils, but the specific problem presented here is that where the footing rests on a granular layer underlain by a cohesive, possibly weak soil.

The approach to solving for the bearing capacity over a two-layer foundation system is presented in the next section. This is followed by a description of the collapse mechanisms considered in the analysis. Some comments about the solution are given next. Results of calculations are then presented in the form of design charts, and generic examples are given. A comparison with experimental results and other methods is also shown. Final remarks complete the paper.

APPROACH

The kinematical approach of limit analysis is used here. This approach yields the upper bound to the true limit loads, but, once reasonable collapse mechanisms are considered, it yields failure loads that are very close to the true collapse loads on elasto–perfectly plastic bodies. This has been confirmed by comparing the upper-bound results to exact solutions (such as the bearing capacity of weightless soil, and problems in metal-forming mechanics). For the bearing capacity of weightless soil the least upper bound is identical to the exact solution (Shield 1954), while for a ponderable soil (half-space) an exact solution is not known, but the discrepancy between the upper-bound and the slip-line solutions is almost negligible. The slip-line solution in this case can be proved to be the lower bound, provided the soil is restricted to a finite volume (not a half-space) limited by rough boundaries, and deformation is governed by the associative flow rule. Close upper-bound and lower-bound solutions also can be found for ultimate loads over nonhomogeneous clay layers (Michalowski and Shi 1993). The kinematic approach of limit analysis leads to solutions identical to those from the "limit equilibrium" approach so widely accepted in design; the two are equivalent (Mróz and Drescher 1969; Michalowski 1989; Salençon 1990; Drescher and Detournay 1993). The authors chose the kinematic approach as it has more appeal to engineering intuition.

The advantage of the kinematic approach over the static, lower-bound approach, is that it is based on the construction of collapse mechanisms verifiable by experiments or practical experience. In the static approach, however, the stress fields are constructed without any clear relation to the true stress field other than the stress boundary conditions. (Note the difference between the lower-bound approach based on constructing statically admissible stress fields and the limit equilibrium approach where only the global force equilibrium is required.)

Yielding of the soil is described here by the Mohr-Coulomb condition (compression taken as positive)

$$f(\sigma_x, \sigma_z, \tau_{xz}) = (\sigma_x + \sigma_z)\sin\varphi - \sqrt{(\sigma_x - \sigma_z)^2 + 4\tau_{xz}^2} + 2c\cos\varphi = 0 \tag{1}$$

where φ = the internal friction angle; and c = cohesion. The upper layer of the granular soil is described by (1) with $c = 0$, and the strength of the cohesive soil (lower layer) is described by the undrained shear strength equal to c_u ($\varphi = 0$). The deformation is governed by the associative flow rule

$$\dot{\varepsilon}_{ij} = \dot{\lambda}\frac{f(\boldsymbol{\sigma}_{ij})}{\partial\boldsymbol{\sigma}_{ij}}; \quad \dot{\lambda} \geq 0,\ i, j = 1, 2, 3 \tag{2}$$

where $\dot{\boldsymbol{\varepsilon}}_{ij}$ = the strain rate tensor; $\boldsymbol{\sigma}_{ij}$ = the stress tensor; and $\dot{\lambda}$ = a nonnegative multiplier.

Eq. (2) implies dilatancy for pressure-sensitive granular soil

[1]Assoc. Prof., Dept. of Civ. Engrg., Johns Hopkins Univ., Baltimore, MD 21218.

[2]Grad. Student, Dept. of Civ. Engrg., Johns Hopkins Univ., Baltimore, MD.

Note. Discussion open until October 1, 1995. To extend the closing date one month, a written request must be filed with the ASCE Manager of Journals. The manuscript for this paper was submitted for review and possible publication on August 3, 1993. This paper is part of the ***Journal of Geotechnical Engineering***, Vol. 121, No. 5, May, 1995. ©ASCE, ISSN 0733-9410/95/0005-0421–0428/$2.00 + $.25 per page. Paper No. 6647.

and incompressibility of clays during deformation. Consequently, in rigid-block mechanisms where all deformation takes place along interfaces between blocks (within "rupture layers"), the velocity "jump" between two blocks in granular soil must be inclined at the angle of internal friction φ to the discontinuity, and in clays it must be tangent.

The upper-bound theorem states that *the rate of energy dissipation is larger than or equal to the rate of work done by external forces in any kinematically admissible mechanism.* Thus, if the material properties and geometry of a collapse mechanism are known, one can find an upper bound to the true limit load through equating the rate of work of external forces to the rate of internal energy dissipation. Optimization of the geometrical parameters in the failure mechanism provides the best approximation of the collapse load (least upper bound).

COLLAPSE MECHANISMS

Due to limited space, considerations are restricted here to a case of practical importance when a layer of granular soil is underlain by a cohesive, possibly weak, material. A symmetrical half of the first of the mechanisms considered is shown in Fig. 1(a). The mechanism is constructed in such a way that the velocity discontinuities originating at point A are bent at the interface between the layers. The angle at which they bend is equal to the difference in the internal friction angle of the soils in the two layers. The velocity-jump vector along segment AG_2, for instance, is then parallel to that along G_2D_2. Their magnitudes are also the same, and block $AG_2D_2D_3G_3A$ moves as one rigid body with velocity V_2. The hodograph for the entire mechanism is shown in Fig. 1(b). A similar mechanism was anticipated by Karal (1979). No analysis or numerical results were offered by Karal, however.

For the mechanism in Fig. 1, the rate of work by the unknown traction under half of the footing is equal to $\bar{p}V_0B/2$ (V_0 being the magnitude of the vertical velocity of the footing). The upper-bound theorem is used to calculate the average limit pressure $\bar{p}$ along boundary OA, with traction q given along AF. The upper bound to the average traction $\bar{p}$ can be written as

$$\bar{p} = \frac{2}{BV_0}\left[\int_v \boldsymbol{\sigma}_{ij}\dot{\boldsymbol{\varepsilon}}_{ij}\,dv - \int_S \mathbf{q}_i\mathbf{V}_i\,dS - \int_v \boldsymbol{\gamma}_i\mathbf{V}_i\,dv\right] \quad (3)$$

where $\dot{\boldsymbol{\varepsilon}}_{ij}$ and $\mathbf{V}_i$ = the strain rate tensor and velocity vector in the kinematically admissible mechanism of collapse; $\boldsymbol{\sigma}_{ij}$ = the stress tensor; $\mathbf{q}_i$ = the known traction vector on boundary S (here AF); $\boldsymbol{\gamma}_i$ = the unit weight vector; and v = volume of the collapsing mass. The first integral in (3) represents the rate of energy dissipation in the mechanism (discontinuities included in volume v), the second one shows the rate of work of a given traction on boundary S (AF), and the last one represents the work rate of the soil weight.

The mechanism consists of rigid blocks, and the energy is dissipated in the shear layers between the blocks. The total rate of energy dissipation in the mechanism [first integral in (3)] was calculated as the sum of dissipation along all discontinuities. Since the associative flow rule is used, the dissipation rate along the velocity discontinuities in the granular material is zero, and in clay ($\varphi = 0$) it is equal to the product of the shear strength and the magnitude of the velocity-jump vector (dissipation per unit area of the discontinuity surface). More specifically, (3) can be written, for the mechanism in Fig. 1, in form

$$\bar{p} = \frac{2}{BV_0}\left[c_u\sum_{j=1}^{m}[V]_j l_j - q\overline{\mathrm{AF}}V_n - \gamma\sum_{k=1}^{n}A_k V_k\right] \quad (4)$$

where l_j = length of the jth velocity discontinuity in clay (for instance, G_1D_1, D_1D_2, etc.); $[V]_j$ = magnitude of the velocity-jump vector along that discontinuity; m = number of straight-line discontinuity segments; V_k = vertical component of the velocity of the kth block (negative if upward); A_k = area of the kth block within the sand layer only; and n = number of blocks (c_u is undrained shear strength of clay; γ is unit weight of sand). All velocities can be obtained from geometrical relations in the hodograph in Fig. 1(b).

The second collapse mechanism is shown in Fig. 2(a). This mechanism is also symmetrical, with blocks AGDOA and AGEJA moving as rigid bodies, and with region GDE deforming in a continuous fashion. The failure pattern in clay resembles that in the classical Prandtl mechanism, and the energy dissipation rate [first integral in (3)] now includes dissipation both along discontinuities and within the continually deforming region GDE.

In addition to the two mechanisms shown in Figs. 1 and 2, a one-sided collapse pattern and a failure mechanism confined to the top layer only [similar to that in Michalowski (1993)] were considered. The objective of the calculations was to obtain the least upper bound to the bearing capacity, and each of the mechanisms considered is a kinematically admissible failure pattern. It was not clear prior to calculations, however, which mechanism would predict the minimum bearing capacity (best upper bound), and all four different mechanisms were considered in order not to predefine the collapse mode. For all cases analyzed here, either the mechanism in Fig. 1 or the mechanism in Fig. 2 ensured the minimum limit load; therefore, the other two mechanisms mentioned are not presented here.

COMMENTS ON SOLUTION

The results of calculations are presented in the next section. Here, however, some consideration is given to the feasibility of presenting the results in terms of traditional bearing capacity coefficients. Also, it is indicated when a weak clay underlying a granular soil has an adverse effect on the bearing capacity.

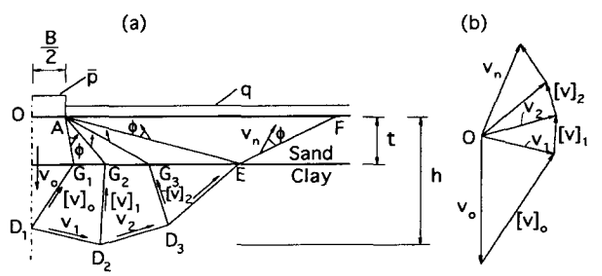

FIG. 1. Collapse Mechanism: (a) Rigid-Block Collapse Mechanism of Two-Layer Foundation Soil; and (b) Hodograph

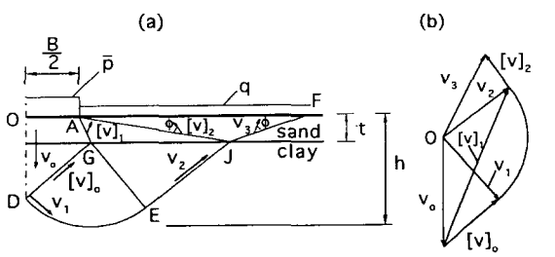

FIG. 2. Collapse Mechanism: (a) Failure Mechanism with Continual Deformation Field in Clay; and (b) Hodograph

Bearing Capacity Coefficients

It follows from the incompressibility of clay and the geometry of the problem considered that the net work done by the weight of the clay must be zero. The solution to the bearing capacity must then be independent of the specific weight of the clay. Dimensional analysis allows one to conclude that the bearing capacity for the two-layer foundation soil can be represented as

$$\frac{\bar{p}}{\gamma B} = f\left(\frac{t}{B}, \frac{c_u}{\gamma B}, \frac{q}{\gamma B}, \varphi\right) \tag{5}$$

where $\bar{p}$ = average limit pressure under the footing; B = footing width; t = thickness of the sand layer; γ and φ = the unit weight and the internal friction angle of the sand, respectively; c_u = undrained shear strength of the clay; and q = surcharge load at the boundary adjacent to the footing [Fig. 1(a)]. Solutions based on (3) can be written as

$$\frac{\bar{p}}{\gamma B} \le \frac{c_u}{\gamma B} f_1 + \frac{q}{\gamma B} f_2 + f_3 = \frac{c_u}{\gamma B} N_c + \frac{q}{\gamma B} N_q + N_\gamma \tag{6}$$

The inequality sign in (6) indicates that the solution yields the upper bound to $\bar{p}/\gamma B$ [as do all solutions based on the consistent limit force equilibrium method, e.g., Terzaghi 1943)]. By comparing (5) and (6) one concludes that f_i are not necessarily functions of the internal friction angle alone, as suggested in bearing capacity formulas for uniform soils. For instance, f_1 and f_3 (N_c, N_γ) for the case where $q = 0$ and $\varphi = 35°$ are shown in Fig. 3 for different t/B, as functions of $c_u/\gamma B$. These functions were calculated from the specific terms in (3) applied to the optimized collapse mechanisms, where a minimum of bearing pressure was sought, and independent angles describing the geometry of the mechanism were variable. Coefficient N_c drops down with an increase in strength of the underlying clay, and, for sufficiently large $c_u/\gamma B$, it becomes zero. This occurs when the entire mechanism of failure is contained within the upper layer of granular material. Coefficient N_γ, on the other hand, increases with an increase in $c_u/\gamma B$, and, when the mechanism becomes restricted to the upper layer, N_γ reaches a value independent of $c_u/\gamma B$ (it is dependent, however, on φ and $q/\gamma B$).

Numerical calculations with optimization of failure mechanisms show that all functions f_i in (6) (which can be interpreted as bearing capacity coefficients N_c, N_q, and N_γ) are dependent on $q/\gamma B$, t/B, $c_u/\gamma B$, and φ. Presentation of these functions would be more elaborate than presentation of the average bearing capacity alone. Therefore, the results are presented in terms of $\bar{p}/\gamma B$ rather than coefficients N_c, N_q, and N_γ.

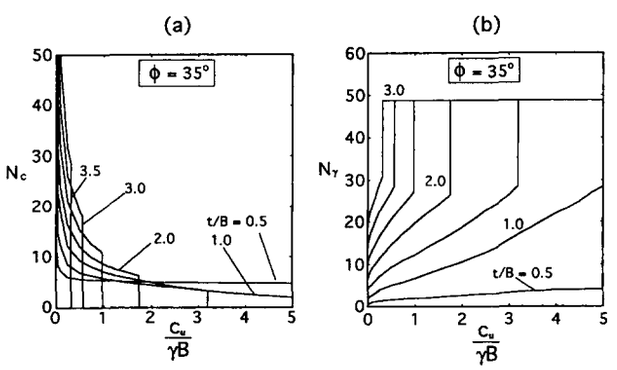

FIG. 3. Bearing Capacity Coefficients as Functions of Cohesion of Underlying Clay for Different Thickness of Sand Layer, t/B, and $q = 0$: (a) Coefficient N_c; and (b) Coefficient N_γ

Critical Depth of Weak Layer

Fig. 4(a) shows the average limit pressure $\bar{p}$ (dotted line) and the depth of the collapse mechanism h, both dependent on the thickness of the sand layer (t/B), for a specific internal friction angle of sand and parameter $c_u/\gamma B$. Cohesive soil weakens the foundation system, but the limit pressure $\bar{p}$ increases when the depth of the clay increases. When this relative depth reaches 2.7 (for this specific case) limit pressure $\bar{p}$ becomes constant, since for greater depths of the clay layer the critical collapse mechanism becomes contained entirely in the upper layer of sand. At $t/B = 2.7$, however, the same least upper bound to $\bar{p}$ is associated with two failure mechanisms: a deep mechanism extending into the clay ($h/B = 3.75$), and a much more shallow mechanism, restricted entirely to the sand layer ($h/B = 1.4$). Fig. 4(a) indicates that, for $\varphi = 40°$, a clay layer with $c_u/\gamma B = 3.0$ is a "weak" soil. It follows from Fig. 4(a) that the depth of the failure mechanism increases with an increase in the depth of the weak clay layer, all other parameters being constant. A weak clay at a certain depth below the footing "attracts" the failure mechanism. However, when parameter $c_u/\gamma B$ is large, the close proximity of the strong clay to the surface increases limit pressure $\bar{p}$ relative to that for the sand alone.

The critical depth of a clay layer is defined here as the largest depth of the clay layer that still has an effect on the limit pressure. For the specific case in Fig. 4(a), the dimensionless parameter (t/B) representing the critical depth is 2.7. Fig. 4(b) shows calculated critical depths for a variety of parameters (but all for a surcharge load equal to zero, $q = 0$). It indicates that the weaker the clay layer, the larger the depth up to which the clay has an adverse effect on the bearing

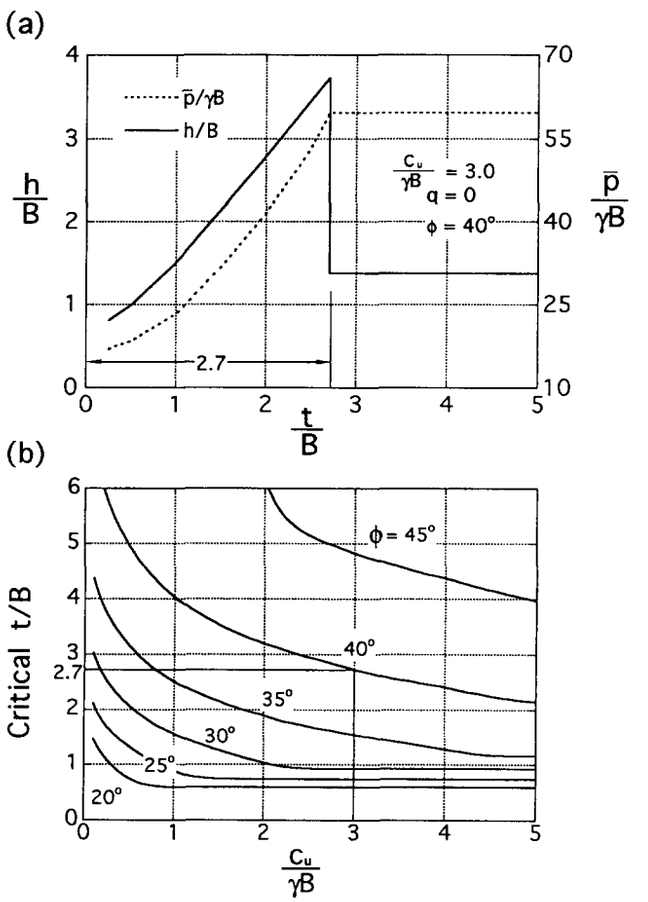

FIG. 4. Critical Depth: (a) Depth of Collapse Mechanism and Limit Pressure as Functions of Thickness of Sand Layer; and (b) Critical Depth of Clay as Function of Clay Shear Strength

capacity of a footing (critical depth). Also, the stronger the sand layer (the larger φ is), the larger the critical depth.

This observation indicates that the often-suggested calculations for estimation of the critical depth of the weak layer as a function of the width of the footing and parameters of the soil immediately under the footing should be abandoned. Calculations such as those suggested in the present paper should be used [for case where $q = 0$ use Fig. 4(b)]. Design charts for bearing pressure $\bar{p}/\gamma B$ given in the next section, however, do not require that the critical depth be calculated first. This critical depth is accounted for in the charts.

DESIGN CHARTS

Results of the calculations are presented in a dimensionless form in Figs. 5–7. All diagrams represent least upper bounds obtained from analyses based on mechanisms in Figs. 1 and 2, whichever yields the minimum. The number of blocks in the mechanism in Fig. 1 used in the calculations was 20. The increase of the number of blocks beyond 20 affected the least upper bound by less than 1%. The independent angles describing the geometry of the mechanism were varied in an optimization scheme (with the smallest angle increment being 0.05°), and (3) was used to calculate the bearing pressure $\bar{p}$ for each combination of these angles. The minimum of $\bar{p}$ was sought.

Dimensionless coefficient $\bar{p}/\gamma B$ representing the average limit pressure under a footing is a function of four parameters, (5), and it cannot be represented conveniently (without making crude approximations) as a function of bearing-capacity coefficients dependent on the internal friction angle alone. Therefore, diagrams for $\bar{p}/\gamma B$ are presented without separating components dependent on cohesion, surcharge load, and the unit weight of the soil (this would require three times more diagrams).

Figs. 5–7 present results for surcharge load $q/\gamma B$ equal to 0, 0.5, and 1.0, respectively. Results are independent of the unit weight of the clay; γ is the unit weight of the granular soil, φ is its internal friction angle ($\varphi = 0$ for clay), and c_u is the undrained shear strength of the clay (no cohesion in the upper layer). In each figure separate diagrams are shown for the internal friction angle of the upper layer: 30°, 35°, 40°, and 45°. The separate curves on the diagrams represent the dependence of the average limit pressure on the shear strength of the clay for a single depth of the clay soil. These curves are shown for different t/B in the range from 0 to 5.5 in 0.5 increments.

A weak clay layer at a relatively shallow depth always has an adverse effect on the bearing capacity. As expected, the limit pressure increases with an increase in the strength of the clay and with an increase in the clay depth. For most cases the limit pressure reaches a constant value and further increase in the clay strength does not improve the bearing capacity. This limit is equal to the bearing capacity of the granular soil alone. Only when the clay is strong and the layer of sand overlying the clay is thin relative to the footing width can the bearing capacity increase beyond that expected for a homogeneous granular soil [see Fig. 5(a) and (b), and Fig. 6(a)]. In such cases the bearing pressure reaches a higher constant level at large $c_u/\gamma B$ (beyond $c_u/\gamma B$ shown in diagrams here). In the case when $t = 0$, the bearing capacity increases proportionally to the clay strength.

The critical depth is implicitly included in the diagrams in Figs. 5–7. If the value of $\bar{p}/\gamma B$ read from these diagrams for a given t/B is less than the limit set by the granular soil alone (horizontal lines), it implies that this specific t/B is less than the critical depth. If the value read from the diagrams is equal to the constant limit independent of $c_u/\gamma B$, the specific t/B is larger or equal to the critical depth. Using the charts in Figs. 5–7 does not require estimation of the critical depth.

The following two examples show the application of the charts in Figs. 5–7 in the design of footings.

Example 1

Find the bearing capacity per unit length of a 2-m wide ($B = 2$ m) strip footing placed on the surface of a 4-m layer ($t = 4$ m) of sand ($\varphi = 35°$, $\gamma = 17$ kN/m^3). The sand layer rests on clay whose undrained shear strength is $c_u = 50$ kN/m^2. From Fig. 5 for $\varphi = 35°$, $c_u/\gamma B \approx 1.5$ and $t/B = 2$, we obtain $\bar{p}/\gamma B = 22.5$, hence the average limit pressure $\bar{p} = 765$ kN/m^2 (calculations using the computer program: $\bar{p} = 764.16$ kN/m^2). The bearing capacity is then equal to $\bar{p}B = 765 \times 2 = 1{,}530$ kN/m.

Example 2

Find the bearing capacity of a 4-m wide strip footing placed at a depth of 2 m ($D = 2$ m) in a 12-m deep layer of sand ($t = 12 - D = 10$ m) with $\varphi = 42°$ and $\gamma = 17.5$ kN/m^3. The clay beneath the sand has an undrained shear strength of $c_u = 105$ kN/m^2. The surcharge load is $q = \gamma D = 35$ kN/m^2 and $q/\gamma B = 0.5$; $c_u/\gamma B = 1.5$ and $t/B = 2.5$. From Fig. 6: for $\varphi = 35°$, $\bar{p}/\gamma B = 36\ (\pm 1)$; for $\varphi = 40°$, $\bar{p}/\gamma B = 45\ (\pm 1)$; and for $\varphi = 45°$, $\bar{p}/\gamma B = 57\ (\pm 1)$. Both parabolic and linear interpolation were tried to find out whether simple linear interpolation is acceptable for practical purposes. Parabolic interpolation for $\varphi = 42°$ yields $\bar{p}/\gamma B = 49.44$, thus the average limit pressure $\bar{p} = 3{,}461\ (\pm 70)$ kN/m^2. Linear interpolation yields: $\bar{p}/\gamma B = 49.80$ and $\bar{p} = 3{,}486\ (\pm 70)$ kN/m^2. Calculations using the computer program for $\varphi = 42°$ gave $\bar{p} = 3{,}432$ kN/m^2 (the maximum depth of the failure mechanism calculated by the program was 20.74 m). It is concluded that linear interpolation in the range of φ from 30° to 45° within 5° steps is acceptable.

COMPARISON TO OTHER METHODS

The method for calculations of the bearing capacity of a two-layer foundation soil suggested by Hanna and Meyerhof (1980) is perhaps the most widely known, and is therefore used here for comparison. Fig. 8 presents the comparison of the average limit pressure calculated using the proposed method to the experimental tests performed by Meyerhof and Hanna (1978) on a model of a footing ($B = 0.05$ m), and to calculations based on design charts presented by Hanna and Meyerhof (1980). Calculations were performed for the internal friction angle of the sand layer equal to 47.5° (from direct shear) and undrained shear strength of clay $c_u = 10$ kN/m^2, as reported by Meyerhof and Hanna (1978), and $\gamma = 16.3$ kN/m^3. It is rather unexpected that the upper-bound solution, for all test points but one, yields a bearing capacity lower than that of the actual experiment (this may be due to influence of the surface friction on walls of the test tank). Small discrepancies between the proposed method and the laboratory tests indicate that the method should prove useful as a design tool.

Further comparison of the computational results is presented in Fig. 9. The method presented here requires no additional concepts [such as a "coefficient of punching shear" (Hanna and Meyerhof 1980)] beyond the standard Mohr-Coulomb yield condition and the flow rule, and the design charts presented (Figs. 5–7) are convenient to use. The differences in results from the two methods (Fig. 9) originate from consideration of different collapse mechanisms and different approach to calculations (optimization). The mechanism used by Hanna and Meyerhof (1980), when considered

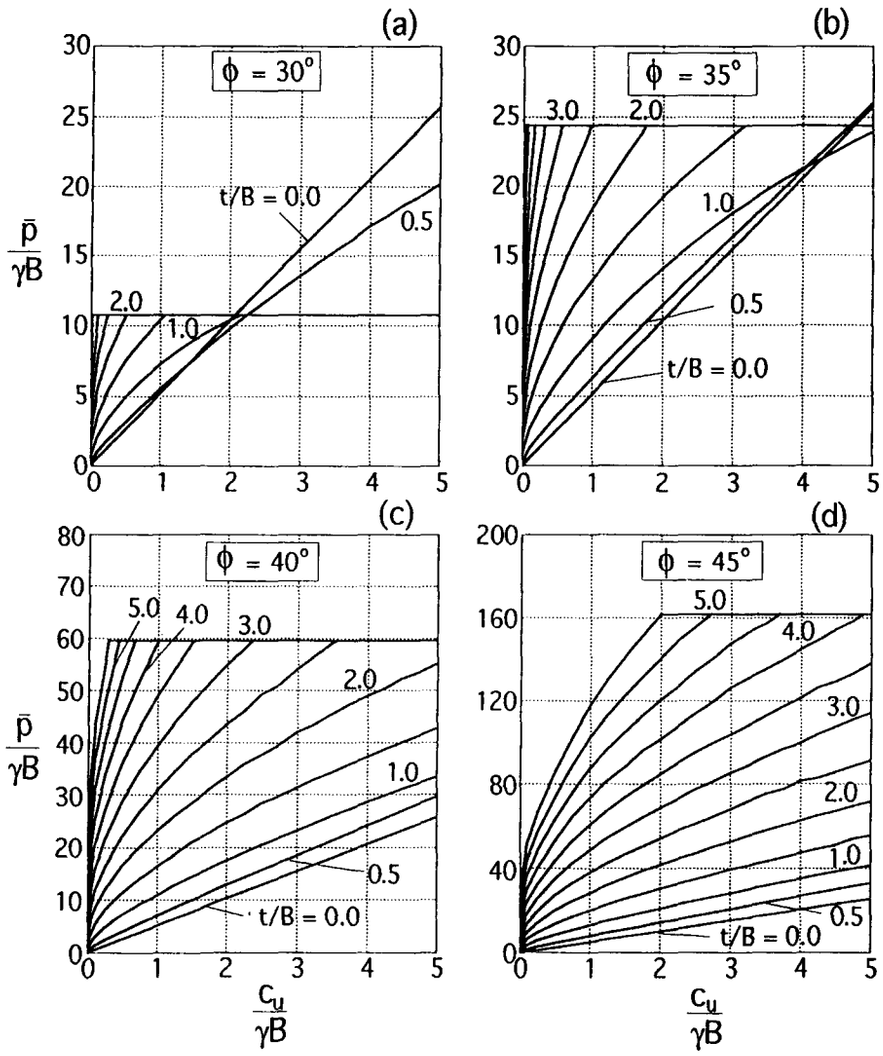

FIG. 5. Dimensionless Limit Pressure on Sand-Clay Foundation Soil, Surcharge Load $q/\gamma B = 0$: (a) $\varphi = 30°$; (b) $\varphi = 35°$; (c) $\varphi = 40°$; and (d) $\varphi = 45°$

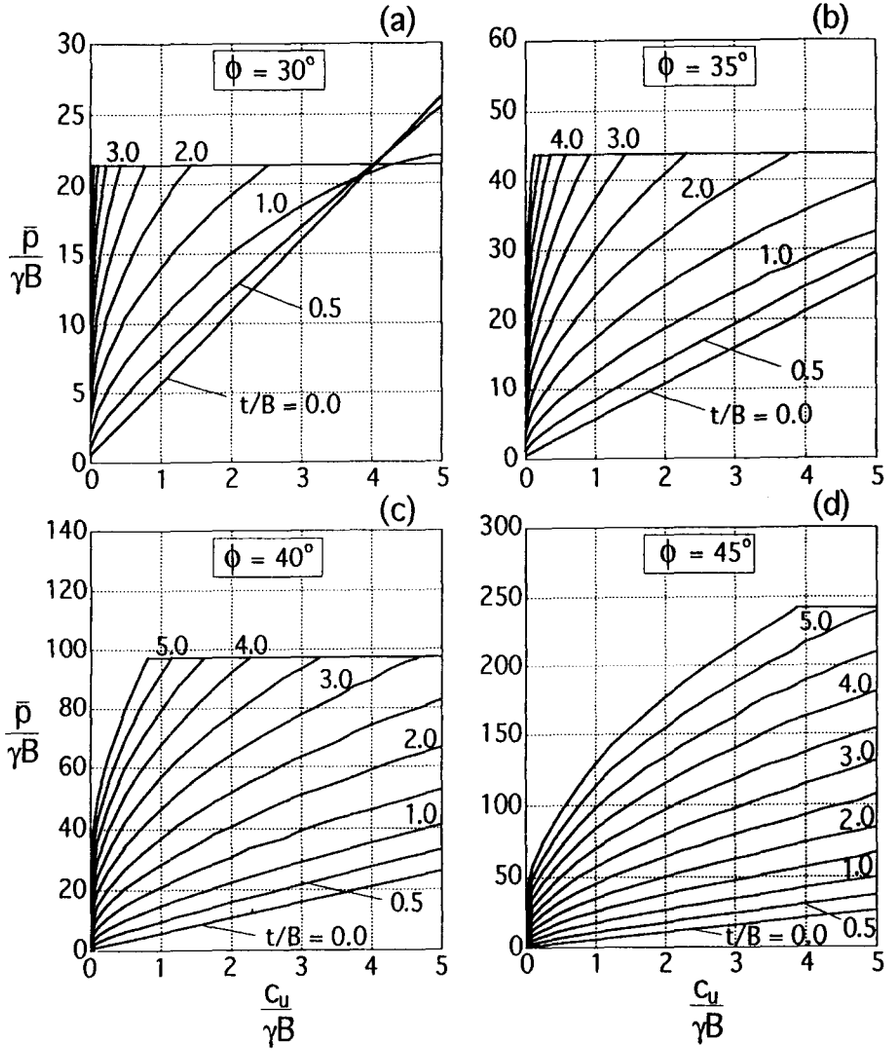

FIG. 6. Dimensionless Limit Pressure on Sand-Clay Foundation Soil, Surcharge Load $q/\gamma B = 0.5$: (a) $\varphi = 30°$; (b) $\varphi = 35°$; (c) $\varphi = 40°$; and (d) $\varphi = 45°$.

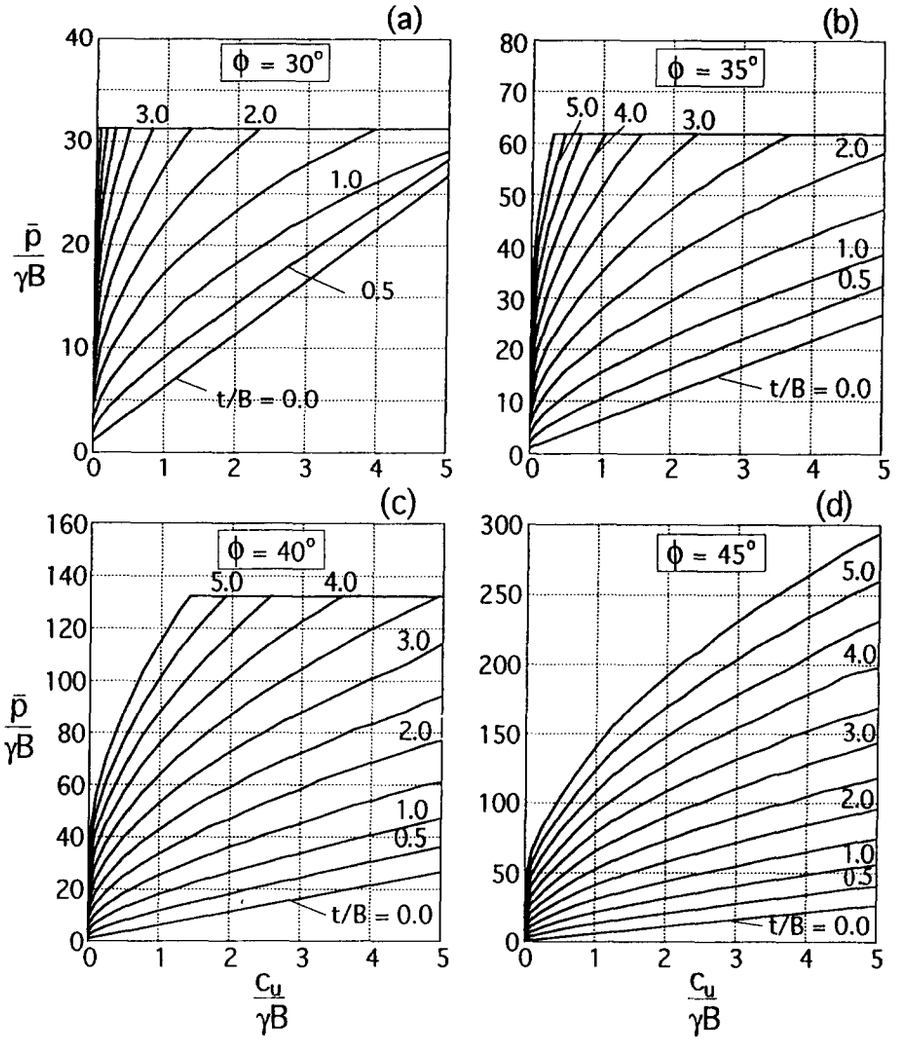

FIG. 7. Dimensionless Limit Pressure on Sand-Clay Foundation Soil, Surcharge Load $q/\gamma B = 1.0$: (a) $\varphi = 30°$; (b) $\varphi = 35°$; (c) $\varphi = 40°$; and (d) $\varphi = 45°$

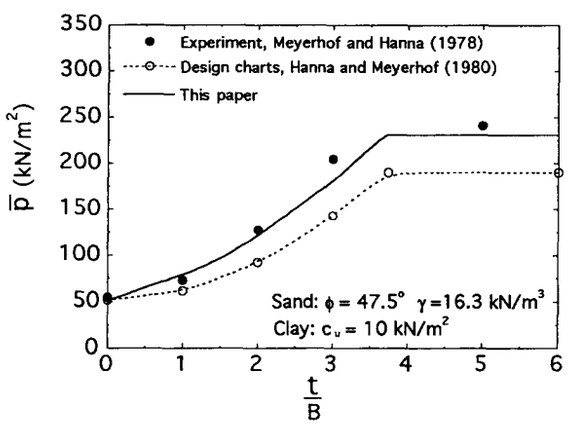

FIG. 8. Comparison of Computational Results to Experimental Tests for Footings with $B = 0.05$ m and $q = 0$

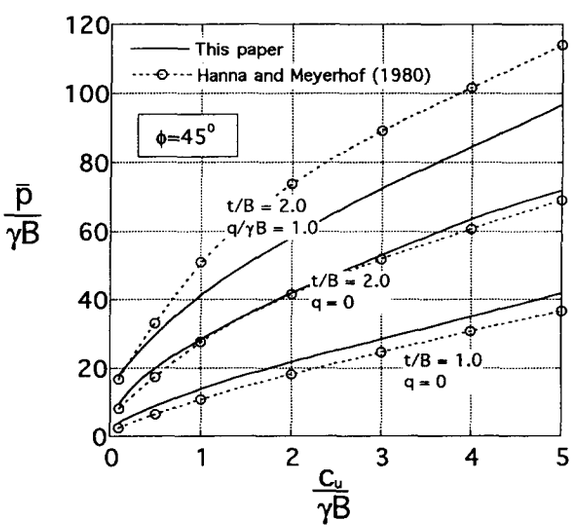

FIG. 9. Comparison of Computational Results

in view of the flow rule in (2), is kinematically inadmissible. This leads to conservative estimates with respect to the rigorous upper-bound calculations, for some combinations of parameters (see curves $t/B = 1.0$ in Fig. 9). Overestimation of the bearing capacity by Hanna and Meyerhof (1980) beyond upper bounds calculated here (for other combinations of parameters; curves for $t/B = 2.0$, $q/\gamma B = 1.0$), is due to not allowing for adjustments of the collapse mechanism (optimization) in calculations of the least bearing capacity.

The design charts presented in Figs. 5–7 were derived under the assumption that the deformation of the sand layer is governed by the associative flow law (normality rule). It can be

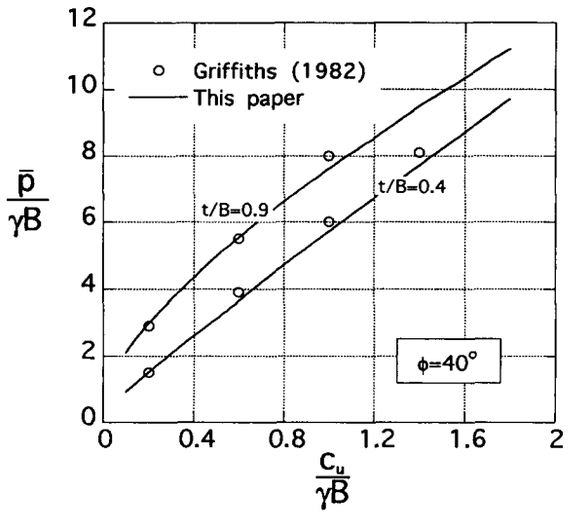

FIG. 10. Comparison of Bearing Pressure Calculations to Finite-Element Computations (Nonassociative Flow Rule)

argued that the normality rule does not accurately describe the deformation of the granular soil, and a nonassociative law should be used for sand. Such law can be described by (2) with the failure function $f(\sigma_{ij}) = 0$ replaced by a plastic potential, say, $g(\sigma_{ij}) = 0$. Further, function $g(\sigma_{ij}) = 0$ can be taken in form of the Mohr-Coulomb function, (1), where the internal friction angle φ is replaced by the dilatancy angle ψ (Davis 1968). Theoretical considerations (Drescher and Detournay 1993) allow one to conclude that for such a nonassociative model of sand ($c = 0$) a solution can be obtained using the same technique as presented herein, but with the internal friction angle φ replaced by angle φ^* calculated from

$$\tan \varphi^* = \frac{\cos \psi \sin \varphi}{1 - \sin \psi \sin \varphi} \tag{7}$$

Fig. 10 shows the comparison of bearing capacities calculated by Griffiths (1982) using the finite-element method, assuming the sand is incompressible ($\psi = 0$), with the ones calculated using the design charts presented here [angle φ^* calculated from (7)]. The two coincide remarkably well.

FINAL REMARKS

A method was presented for calculations of the bearing capacity of strip footings over a two-layer foundation soil system. Design charts are shown for the case where a layer of granular soil overlies the cohesive soil, either weak or strong. The method can be applied easily to a general case where the strengths of both layers are characterized by both internal friction and cohesion.

The formulation of the bearing-capacity problem and the solution using the upper-bound theorem of limit analysis is conceptually straightforward. The solution does not require introducing concepts or assumptions [such as the "coefficient of punching shear" (Hanna and Meyerhof 1980)] used in some limit equilibrium approaches to avoid statical indeterminacy. The advantage of the upper-bound approach is in the clarity of the concept and the small effort needed to generalize the solution to include both friction and cohesion in both layers, inclined loads, and so on.

The simplicity of the solution to the relatively complicated problem of the bearing capacity of footings over two different soils was achieved by introducing a failure mechanism where the velocity discontinuities were bent at specific angles at the interface between layers. This allowed one to construct a simple hodograph, as in the case of a uniform soil. Optimization of the geometry of the mechanism led to the least upper bounds. It was found, however, that, for a strong first layer (large φ) and weak underlying clay, a mechanism with a continual deformation field in the weak layer was more effective.

The collapse mechanism that assures the least upper bound to the bearing capacity can attain a very large depth, far exceeding that for homogeneous soils. This depth becomes particularly large for a strong granular layer (high internal friction angle) and a weak clay underneath.

ACKNOWLEDGMENT

The results presented in this paper are based on work supported by the National Science Foundation under grant No. MSS9301494. This support is gratefully acknowledged.

APPENDIX I. REFERENCES

Bowles, J. E. (1988). *Foundation analysis and design*, 4th Ed., McGraw-Hill, New York, N.Y.

Chen, W. F., and Davidson, H. L. (1973). "Bearing capacity determination by limit analysis." *J. Soil Mech. Found. Div.*, 99(6), 433–449.

Davis, E. H. (1968). "Theories of plasticity and the failure of soil masses." *Soil mechanics: selected topics*, I. K. Lee, Ed., Butterworth, London, England, 341–380.

Drescher, A., and Detournay, E. (1993). "Limit load in translational failure mechanisms for associative and non-associative materials." *Géotechnique*, London, England, 43(3), 443–456.

Florkiewicz, A. (1989). "Upper bound to bearing capacity of layered soils." *Can. Geotech. J.*, 26(4), 730–736.

Griffiths, D. V. (1982). "Computation of bearing capacity on layered soil." *Proc., 4th Int. Conf. Num. Meth. Geomech.*, Z. Eisenstein, Ed., Balkema, Rotterdam, The Netherlands, 163–170.

Hanna, A. M., and Meyerhof, G. G. (1980). "Design charts for ultimate bearing capacity of foundations on sand overlying soft clay." *Can. Geotech. J.*, 17(2), 300–303.

Hansen, J. B. (1970). "A revised and extended formula for bearing capacity." *Geoteknisk Inst., Bull.*, 28, 5–11.

Karal, K. (1979). "Energy method for soil stability analysis," PhD thesis, Norwegian Institute of Technology, Trondheim, Norway.

Meyerhof, G. G. (1974). "Ultimate bearing capacity of footings on sand layer overlying clay." *Can. Geotech. J.*, 11(2), 223–229.

Meyerhof, G. G., and Hanna, A. M. (1978). "Ultimate bearing capacity of foundations on layered soils under inclined load." *Can. Geotech. J.*, 15(4), 565–572.

Michalowski, R. L. (1989). "Three-dimensional analysis of locally loaded slopes." *Géotechnique*, London, England, 39, 27–38.

Michalowski, R. L. (1993). "Limit analysis of weak layers under embankments." *Soils and Fond.*, 33(1), 155–168.

Michalowski, R. L., and Shi, L. (1993). "Bearing capacity of nonhomogeneous clay layers under embankments." *J. Geotech. Engrg.*, ASCE, 119(10), 1657–1669.

Mróz, Z., and Drescher, A. (1969). "Limit plasticity approach to some cases of flow of bulk solids." *J. Eng. Ind.*, 51(2), 357–364.

Prandtl, L. (1920). "Über die Härte plastischer Körper." *Nachr. Ges. Wissensch, Göttingen, math.-phys. Klasse*, 74–85 (in German).

Reddy, A. S., and Srinivasan, R. J. (1967). "Bearing capacity of footings on layered clays." *J. Soil. Mech. Found. Div.*, ASCE, 93(2), 83–99.

Reissner, H. (1924). "Zum Erddruckproblem." *Proc., First Int. Congr. for Appl. Mech.*, C. B. Biezeno and J. M. Burgers, Eds., Technische Boekhandel en Drukkerii J. Waltman Jr., The Netherlands, Delft, 295–311.

Salençon, J. (1990). "An introduction to the yield design theory and its applications to soil mechanics." *Eur. J. Mech., Ser. A/Solids*, 9(5), 477–500.

Shield, R. T. (1954). "Plastic potential theory and Prandtl bearing capacity solution." *J. Appl. Mech.*, 21(2), 193–194.

Terzaghi, K. (1943). *Theoretical soil mechanics*. J. Wiley & Sons, New York, N.Y.

APPENDIX II. NOTATION

The following symbols are used in this paper:

B = width of footing;
c_u = undrained shear strength of clay;

D = depth of footing;
$f(\boldsymbol{\sigma}_{ij})$ = yield condition;
f_i = bearing capacity functions ($i = 1, 2, 3$);
h = depth of failure mechanism;
N_c, N_q, N_γ = bearing capacity coefficients;
$\bar{p}$ = average limit pressure (bearing pressure);
q = overburden pressure (γD);
t = thickness of sand layer or depth of clay;
$\mathbf{V}_i$ = velocity vector;
γ = unit weight of sand;
$\dot{\boldsymbol{\varepsilon}}_{ij}$ = strain rate tensor;
$\boldsymbol{\sigma}_{ij}$ = stress tensor;
φ = internal friction angle of sand; and
ψ = dilatancy angle of sand.